Electronic Supplementary Information (ESI)

Robust Lanthanide Metal–Organic Frameworks with "All-in-One" Multifunction: Efficient Gas uptake and Separation, Tunable Light Emission and Luminescent Sensing

Bo Li,*[a] Jian-Peng Dong,[a] Zhe Zhou,[b] Rui Wang,*[b] Li-Ya Wang,*[a] and Shuang-Quan Zang[b]

[a.]College of Chemistry and Pharmaceutical Engineering, Nanyang Normal University, Nanyang 473061, People's Republic of China.

[b.]College of Chemistry, Zhengzhou University, Zhengzhou 450001, People's Republic of China.

Corresponding authors:

*(B. Li) E-mail: libony0107@nynu.edu.cn

*(L. Y. Wang) E-mail: wly@nynu.edu.cn

*(R. Wang) E-mail: wangruijy@zzu.edu.cn

Materials and Instrumentations

All of the materials for syntheses were commercially available and used without further purification. All the solvents used were of analytical grade. Powder X-ray diffraction (PXRD) data of the samples were collected on a D/MAX-3D diffractometer with Cu Kα radiation (λ=1.5418 Å) over the 2θ range of 3°–50° at the scan rate of 5° min^{-1} at room temperature. Simulation of the PXRD spectra was carried out with the single-crystal data and diffraction crystal module of the Mercury program available free of charge via http://www.ccdc. cam.ac.uk/mercury/. Thermogravimetry analyses (TGA) were performed on a TA Q50 system under a N_2 atmosphere (flow rate = 60 mL min^{-1}) in the temperature range 25-700 °C at a heating rate of 10 °C min^{-1}. Elemental analyses of C, H and N for all samples were collected on a Perkin-Elmer 240 analyzer. Inductively coupled plasma (ICP) data were obtained on an ICP-9000(N+M) inductively coupled plasma emission spectrometer. Fourier-transform infrared spectra (FT-IR) were recorded on a Shimadzu IR Tracer-100 by using KBr pellets (4000-400 cm^{-1}). UV-vis diffuse reflectance spectra were recorded with a Shimadzu UV-2600 UV-vis spectrophotometer. Luminescence spectra and lifetime decays were collected on an Edinburgh FLS980 fluorescence spectrophotometer. Time resolved emission spectra (TRES) of the samples were recorded with an Edinburgh FLS 920 with a pulsed xenon lamp as the light source. Quantum efficiency was measured using the integrating sphere on a FluoroMax-4 spectrophotometer. All photographs were taken with a Canon EOS 80D camera.

Experimental Section

Syntheses of $\{[Ln(L)(H_2O)]\cdot 4H_2O\}_n$ (Ln = Eu, Tb, Gd)

A similar procedure was used to obtain all complexes. For the preparation of **1-Eu**, a solution containing H_3L (0.014 g, 0.05 mmol), $Eu(NO_3)_3\cdot 6H_2O$ (0.045 g, 0.1 mmol), DMF (3 mL), H_2O (2 mL) and HNO_3 (1M, 0.5 mL) was stirred for 10 min, and then transferred to a Teflon-lined stainless steel vessel. The vessel was sealed and then heated at 130 °C for 72 h, after cooled to room temperature at a rate of 5 °C min^{-1}, the resulting colorless crystals were harvested by filtration, washed with distilled water, and then dried in air to furnish **1-Eu**. Other complexes were synthesized similarly to **1-Eu**, except that Tb, Gd nitrates ($Ln(NO_3)_3\cdot 6H_2O$ 0.1mmol) in place of Eu(III) nitrate.

$\{[Eu(L)(H_2O)]\cdot 4H_2O\}_n$ (**1-Eu**). Yield: 72.6% (based on H_3L). $C_{14}H_{16}EuNO_{11}$ (Mr = 526.17). Elemental analysis calcd: C 31.93, H 3.07, N 2.66 %. Found: C 32.06, H 3.11, N 2.72 %. IR (KBr pellet, cm^{-1}): 3360 (w), 2359 (w), 1601 (m), 1545 (s), 1459 (m), 1376 (s), 1267 (s), 1036 (m), 870 (m), 832 (m), 773 (s), 704 (m), 602 (w), 530 (w), 472 (m).

$\{[Tb(L)(H_2O)]\cdot 4H_2O\}_n$ (**1-Tb**). Yield: 69.5% (based on H_3L). $C_{14}H_{16}TbNO_{11}$ (Mr = 533.13). Elemental analysis calcd: C 31.51, H 3.02, N 2.63 %. Found. C 31.57, H 3.13, N 2.68 %. IR (KBr pellet, cm^{-1}): 3349 (w), 2358 (w), 1609 (m), 1551 (s), 1490 (m), 1379 (s), 1269 (s), 1035 (m), 875 (m), 838 (m), 774 (s), 704 (m), 606 (w), 549 (w), 468 (m).

$\{[Gd(L)(H_2O)]\cdot 4H_2O\}_n$ (**1-Gd**). Yield: 68.7% (based on H_3L). $C_{14}H_{16}GdNO_{11}$ (Mr = 531.57). Elemental analysis calcd: C 31.60, H 3.03, N 2.63 %. Found: C 31.76, H 3.08, N 2.71 %. IR (KBr pellet, cm^{-1}): 3351 (w), 2356 (w), 1608 (m), 1551 (s), 1489 (m), 1381 (s), 1270 (s), 1039 (m), 876 (m), 839 (m), 775 (s), 704 (m), 608 (w), 551 (w), 470 (m).

Syntheses of doped bimetallic Eu_xTb_{1-x} MOFs

The synthetic procedure for complex **1-Eu_xTb_{1-x}** was the same as that for compound **1-Eu** except that a mixture of $Eu(NO_3)_3\cdot 6H_2O$ and $Tb(NO_3)_3\cdot 6H_2O$ replaces $Eu(NO_3)_3\cdot 6H_2O$. The total molar amount of Eu^{3+} and Tb^{3+} remained unchanged at 0.1 mmol, and differently doped crystals were obtained by adjusting the molar fraction of Eu^{3+} from 1% to 90%. The powder X-ray diffractions (PXRD) proved the isostructural

structures of the doped complexes to **1-Ln**. The contents of Eu^{3+} and Tb^{3+} in **1-Eu_xTb_{1-x}** were determined by ICP analysis and provided in Table S5.

X-Ray crystallography

Single-crystal X-ray diffraction (SCXRD) measurements were performed on a Rigaku XtaLAB Pro diffractometer with Cu-Kα radiation (λ = 1.54178 Å) at 200/293 K. The SADABS program was used for absorption correction.[1] All the structures were solved by direct methods and refined by the full-matrix least-squares method on F^2 with SHELXS and SHELXL programs.[2] The hydrogen atoms on ligands were placed in calculated positions and refined using the riding model. The hydrogens attached to water molecules were located from the difference Fourier maps and refined isotropically. The final formula of **1-Ln** was determined by means of single-crystal structure, TGA and elemental analysis. Refinement parameters and crystallographic data are listed in Table S1-S4 (Supporting Information).

Gas sorption measurements

The gas sorption isotherms were measured by the Micromeritics ASAP 2020 HD88 system by using high-purity gases (N_2, 99.9999%; C_2H_2, 99.9%; CO_2, 99.999%; CH_4, 99.99%). In order to remove all the guest solvents from **1-Eu**, the fresh sample was guest-exchanged with methanol at least 10 times. Then the sample was activated at 393 K for 10 h with high vacuum (the outgas rate was 5 mmHg min^{-1}) to yield the activated material **1-Eu-a** for further gas sorption studies. The samples were maintained at 77 K by immersing the sample tube in a liquid-nitrogen bath, and at other temperatures (273 K and 298 K) by using a circulating water bath. Cycling C_2H_2/CO_2 adsorption experiment of **1-Eu-a** was carried out under 273 and 298 K, and regenerated at 393 K under dynamic vacuum for 30 minutes.

Calculation of Isosteric Heats of Adsorption

The isosteric heats of adsorption (Q_{st}) were calculated using the Clausius-Clapeyron equation based on pure-component isotherms collected at two different temperatures of 273K and 298 K. The Q_{st} was defined as

$$Q_{st} = -R\left(\frac{\partial lnP}{\partial\left(\frac{1}{T}\right)}\right)_y$$

Where *P* is the pressure, T is the temperature, R is the gas constant and y is the adsorption amount.[3] These calculations are done through the "Heat of Adsorption" function embedded in the software supplied by Micromeritics 3-Flex Surface Characterization Analyzer.

Fitting of single component adsorption isotherms

The adsorption curves of C_2H_2, CO_2, CH_4 and N_2 at 273/298K were fitted with the dual-site Langmuir-Freundlich (DSLF) equation[4]:

$$q = q_{m1}\frac{b_1P^{\left(\frac{1}{t_1}\right)}}{1 + b_1P^{\left(\frac{1}{t_1}\right)}} + q_{m2}\frac{b_2P^{\left(\frac{1}{t_2}\right)}}{1 + b_2P^{\left(\frac{1}{t_2}\right)}}$$

Here, q is the uptake (mmol g^{-1}), P is the pressure (kPa), q_{m1} and q_{m2} are the saturation uptakes (mmol g^{-1}) for sites 1 and 2, b_1 and b_2 are the affinity coefficients (kPa^{-1}) for sites 1 and 2, and t_1 and t_2 represent the deviations from the ideal homogeneous surface (unit less) for sites 1 and 2. The parameters that were obtained from the fitting of the adsorption isotherms can be found in Tables S1-S2. Figure 4c shows that the DSLF equation fits the single component adsorption isotherms well. All isotherms were fitted with R^2 > 0.999.

IAST calculations

The selectivity $S_{1/2}$ in a binary mixture of components 1 and 2 is defined as

$$S_{ads} = \frac{x_1/x_2}{y_1/y_2}$$

where the x_1 represent the molar loadings of component 1 that is in equilibrium with a bulk gas phase with partial pressures y_1 in the mixture. We calculate the values of x_1 and x_2 using the Ideal Adsorbed Solution Theory (IAST) of Myers and Prausnitz.[5]

Dynamic Gas Breakthrough Experiments

The breakthrough experiments were conducted at ambient conditions (1 bar, 298 K) by using a laboratory-scale fix-bed reactor (Scheme S1). In a typical experiment, 0.6559 g of **1-Eu** powder was packed into a column (length of adsorption bed: 85 mm; inner diameter of adsorption bed: 6 mm). The sample was activated in-situ under pure helium purging at 393 K for 12 hours prior to the experiment. The temperature was precisely controlled using a temperature controller equipped with a heating tape. The flow of He was then turned off while a gas mixture of 50% C_2H_2 and 50% CO_2 at 5 mL min^{-1} was allowed to flow into the column. The composition of gas came out of the column was monitored using an online mass spectrometer (MS). For the cycling experiment, prior to the each cycle, we regenerated the sample by flushing the adsorption bed with helium gas (20 mL min^{-1}) for 60 min at 393 K.

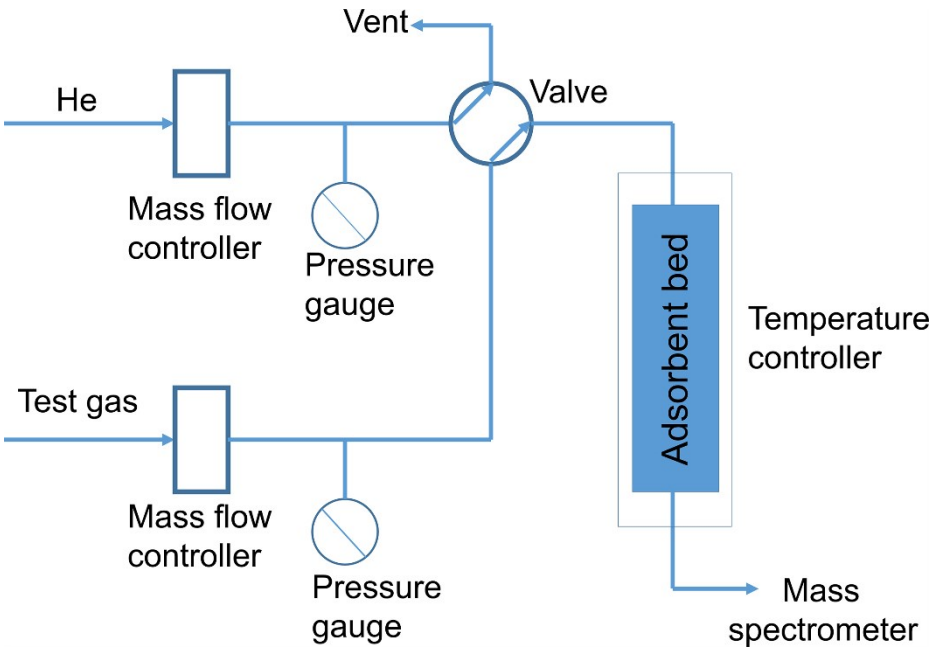

Scheme S1. Schematic illustration of the breakthrough experimental setup.

Calculation method

The present first principle DFT calculations are carried out using the Vienna Ab initio Simulation Package (VASP)[6] with the projector augmented wave (PAW) method.[7] The generalized gradient approximation (GGA) of Perdew-Burke-Ernzerhof (PBE)[8] functional is used to describe the exchange functional. The energy cutoff for the plane wave basis expansion was set to 450 eV and the force on each atom less than 0.03 eV/Å was set for convergence criterion of geometry relaxation. The Brillouin-zone integration was

sampled by single Gamma point. The self-consistent calculations apply a convergence energy threshold of 10^{-4} eV. The DFT-D3 method was employed to consider the van der Waals interaction.[9]

The binding energy was calculated according to:

$E_{binding} = E_{total} - E_{MOF} - E_{gas}$

Where E_{total} is the total energy of the gas molecule adsorbed system, E_{MOF} and E_{gas} are the energies of the pure MOF structure and the gas molecule, respectively.

Luminescence Sensing Experiments

The luminescent sensing experiments for **1-Eu** were completed at room temperature. In particular, 2.0 mg of powder sample was added into 3.0 mL of deionized water of $M(NO_3)_x$ (M = K^+, Na^+, Pb^{2+}, Mn^{2+}, Zn^{2+}, Al^{3+}, Hg^{2+}, Ag^+, Fe^{2+}, Bi^{3+}, Cr^{3+}, Co^{2+}, Ni^{2+}, Cd^{2+}, Ca^{2+}, Cu^{2+}, Mg^{2+}, and Fe^{3+}) and KX (X = PO_4^{3-}, NO_3^-, SCN^-, IO_3^-, Br^-, CO_3^{2-}, $H_2PO_4^-$, MnO_4^-, SO_3^{2-}, SO_4^{2-}, OH^-, Ac^-, Cl^-, I^-, CrO_4^{2-}, $Cr_2O_7^{2-}$) at the same concentration (1 mM). Then, the mixtures were ultrasonicated for 10 min to form a suspension, followed by recording of the luminescent spectra under the same conditions.

Table S1. Crystal data and structural refinement parameters for **1-Eu, 1-Tb and 1-Gd.**

	1-Eu	**1-Tb**	**1-Gd**
CCDC number	2005957	2005958	2005959
Formula	$C_{14}H_{16}EuNO_{11}$	$C_{14}H_{16}TbNO_{11}$	$C_{14}H_{16}GdNO_{11}$
Formula weight	526.24	533.20	531.53
T / K	200(2)	293(2)	200(2)
λ / Å	1.54178	1.54178	1.54178
Space group	$P4_3$	$P4_3$	$P4_3$
Crystal system	Tetragonal	Tetragonal	Tetragonal
a / Å	12.35620(10)	12.396	12.32110(10)
b / Å	12.35620(10)	12.396	12.32110(10)
c / Å	14.7154(2)	14.60440(10)	14.6636(2)
α / deg	90	90	90
β / deg	90	90	90
γ / deg	90	90	90
V / Å^3	2246.68(5)	2244.124(15)	2226.07(5)
Z	4	4	4
D_{calc} (g cm^{-3})	1.556	1.578	1.586
μ / mm^{-1}	20.437	15.950	19.727
Reflections collected	6438	25253	6371
Independent reflections	3522	3981	3498
R(int)	0.0304	0.0305	0.0291
F(000)	1032	1040	1036
GOF on F^2	1.096	1.034	1.048
R_1[a] [$I > 2\sigma(I)$]	0.0360	0.0320	0.0347
wR_2[b] (all data)	0.1012	0.0949	0.0964

$^{a}R_1 = \Sigma||F_o| - |F_c||/\Sigma|F_o|$. $^{b}wR_2 = [\Sigma w(F_o^2 - F_c^2)^2/\Sigma w(F_o^2)^2]^{1/2}$.

Table S2. Selected bond lengths (Å) and angles (°) for **1-Eu**.

Eu1-O1	2.528(6)	Eu1-O2	2.404(6)	Eu1-O3A	2.310(5)
Eu1-O4B	2.353(5)	Eu1-O5C	2.568(6)	Eu1-O6C	2.644(6)
Eu1-O6D	2.480(6)	Eu1-O1W	2.425(6)	Eu1-N1D	2.585(7)
O3A-Eu1-O4B	142.7(2)	O3A-Eu1-O2	89.7(2)	O4B-Eu1-O2	84.9(2)
O3A-Eu1-O1W	80.4(2)	O4B-Eu1-O1W	77.3(2)	O2-Eu1-O1W	134.1(2)
O3A-Eu1-O6D	71.91(19)	O4B-Eu1-O6D	141.29(19)	O2-Eu1-O6D	77.2(2)
O1W-Eu1-O6D	138.3(2)	O3A-Eu1-O1	70.8(2)	O4B-Eu1-O1	76.7(2)
O2-Eu1-O1	53.0(2)	O1W-Eu1-O1	81.7(2)	O6D-Eu1-O1	116.1(2)
O3A-Eu1-O5C	78.00(19)	O4B-Eu1-O5C	125.19(19)	O2-Eu1-O5C	143.1(2)
O1W-Eu1-O5C	78.5(2)	O6D-Eu1-O5C	65.85(19)	O1-Eu1-O5C	145.3(2)
O3A-Eu1-N1D	134.9(2)	O4B-Eu1-N1D	80.2(2)	O2-Eu1-N1D	79.6(2)
O1W-Eu1-N1D	136.3(2)	O6D-Eu1-N1D	63.06(2)	O1-Eu1-N1D	128.3(2)
O5C-Eu1-N1D	84.9(2)	O3A-Eu1-O6D	123.6(18)	O4B-Eu1-O6D	76.03(18)
O2-Eu1-O6D	144.06(19)	O7-Eu1-O6D	71.04(18)	O6C-Eu1-O6D	99.05(16)
O1-Eu1-O6D	144.9(2)	O5C-Eu1-O6D	49.68(17)	N1D-Eu1-O6D	67.45(19)
Symmetry transformations used to generate equivalent atoms: A: *1-y, 1+x, -0.25+z*; B: *-x, 1-y, -0.5+z*; C: *1-x, 1-y, -0.5+z*; D: *1-y, +x, -0.25+z*.					

Table S3. Selected bond lengths (Å) and angles (°) for **1-Tb**.

Tb1-O1	2.364(5)	Tb1-O2	2.516(5)	Tb1-O3A	2.329(4)
Tb1-O4B	2.289(4)	Tb1-O5C	2.537(5)	Tb1-O6C	2.635(5)
Tb1-O6D	2.456(5)	Tb1-O1W	2.394(5)	Tb1-N1D	2.570(5)
O4B-Tb1-O3A	142.86(16)	O4B-Tb1-O1	89.86(18)	O3A-Tb1-O1	85.68(17)
O4B-Tb1-O1W	79.51(17)	O3A-Tb1-O1W	77.61(17)	O1-Tb1-O1W	134.35(17)
O4B-Tb1-O6D	71.53(16)	O3A-Tb1-O6D	141.82(16)	O1-Tb1-O6D	76.73(17)
O1W-Tb1-O6D	137.60(17)	O4B-Tb1-O2	71.22(17)	O3A-Tb1-O2	76.76(16)
O1-Tb1-O2	53.17(16)	O1W-Tb1-O2	81.56(17)	O6D-Tb1-O2	115.87(16)
O4B-Tb1-O5C	77.49(16)	O3A-Tb1-O5C	125.07(16)	O1-Tb1-O5C	142.47(18)
O1W-Tb1-O5C	78.38(19)	O6D-Tb1-O5C	65.76(16)	O2-Tb1-O5C	145.33(18)
O4B-Tb1-N1D	134.85(18)	O3A-Tb1-N1D	80.41(17)	O1-Tb1-N1D	79.43(17)
O1W-Tb1-N1D	136.97(18)	O6C-Tb1-N1D	63.32(16)	O2-Tb1-N1D	128.18(17)
O5C-Tb1-N1D	84.86(18)	O4B-Tb1-O6C	123.28(16)	O3A-Tb1-O6C	75.64(14)
O1-Tb1-O6C	144.70(16)	O1W-Tb1-O6C	71.38(16)	O6D-Tb1-O6C	99.43(13)
O2-Tb1-O6C	144.70(16)	O5C-Tb1-O6C	49.96(14)	N1D-Tb1-O6C	67.53(16)
Symmetry transformations used to generate equivalent atoms: A: *1-x, -y, -0.5+z*; B: *1-y, +x, -0.25+z*; C: *2-x, -y, -0.5+z*; D: *1-y, -1+x, -0.25+z*.					

Table S4. Selected bond lengths (Å) and angles (º) for **1-Gd**.

Gd1-O1A	2.344(5)	Gd1-O2B	2.300(5)	Gd1-O3C	2.387(6)
Gd1-O4C	2.522(6)	Gd1-O5D	2.553(6)	Gd1-O6D	2.630(6)
Gd1-O6	2.475(6)	Gd1-O1W	2.416(6)	Gd1-N1	2.585(7)
O1A-Gd1-O1W	77.47(19)	O1A-Gd1-O2B	142.6(2)	O1W-Gd1-O2B	80.3(19)
O1A-Gd1-O3C	84.94(19)	O1W-Gd1-O3C	133.89(19)	O2B-Gd1-O3C	89.3(2)
O1A-Gd1-O4C	76.36(19)	O1W-Gd1-O4C	81.33(18)	O2B-Gd1-O4C	70.8(2)
O3C-Gd1-O4C	53.01(19)	O1A-Gd1-O5D	125.47(18)	O1W-Gd1-O5D	78.5(2)
O2B-Gd1-O5D	77.95(19)	O3C-Gd1-O5D	143.0(2)	O4C-Gd1-O5D	145.2(2)
O1A-Gd1-O6	141.44(19)	O1W-Gd1-O6	137.9(2)	O2B-Gd1-O6	71.23(18)
O3C-Gd1-O6	77.28(19)	O4C-Gd1-O6	116.35(19)	O5D-Gd1-O6	65.75(18)
O1A-Gd1-O6D	75.77(17)	O1W-Gd1-O6D	71.23(18)	O2B-Gd1-O6D	124.12(18)
O3C-Gd1-O6D	144.01(19)	O4C-Gd1-O6D	144.32(18)	O5D-Gd1-O6D	50.23(17)
O6-Gd1-O6D	99.33(16)	O1A-Gd1-N1	80.1(2)	O1W-Gd1-N1	136.6(2)
O2B-Gd1-N1	135.0(2)	O3C-Gd1-N1	79.6(2)	O4C-Gd1-N1	128.1(2)
O5D-Gd1-N1	85.2(2)	O6-Gd1-N1	63.29(19)	O6D-Gd1-N1	67.48(19)
Symmetry transformations used to generate equivalent atoms: A: *+y, 2-x, 0.25+z*; B: *-1+x, +y, +z*; C: *1-y, +x, -0.25+z*; D: *+y, 1-x, 0.25+z*.					

Table S5. The molar ratios of Eu^{3+} and Tb^{3+} ions and CIE coordinates of doped **1-Eu_xTb_{1-x}**.

1-Eu_xTb_{1-x} (x%)	Eu/Tb (%) ratio used in the reaction	Eu/Tb (%) ratio calculated from ICP		CIE
		Eu^{3+}	Tb^{3+}	
1-$Eu_0Tb_{100\%}$	0:100	0	100	(0.3316,0.5922)
1-$Eu_{1\%}Tb_{99\%}$	1:99	1.08	98.92	(0.3801,0.5510)
1-$Eu_{2\%}Tb_{98\%}$	2:98	1.96	98.04	(0.4166,0.5243)
1-$Eu_{3\%}Tb_{97\%}$	3:97	3.02	96.98	(0.4463,0.5014)
1-$Eu_{4\%}Tb_{96\%}$	4:96	4.05	95.95	(0.4704,0.4848)
1-$Eu_{5\%}Tb_{95\%}$	5:95	5.13	94.87	(0.4861,0.4715)
1-$Eu_{6\%}Tb_{96\%}$	6:94	6.11	93.89	(0.4968,0.4637)
1-$Eu_{7\%}Tb_{93\%}$	7:93	7.06	92.94	(0.5189,0.4452)
1-$Eu_{8\%}Tb_{92\%}$	8:92	8.10	91.90	(0.5369,0.4319)
1-$Eu_{9\%}Tb_{91\%}$	9:91	9.07	90.93	(0.5590,0.4141)
1-$Eu_{10\%}Tb_{90\%}$	10:90	10.56	89.44	(0.5750,0.4015)
1-$Eu_{30\%}Tb_{70\%}$	30:70	29.74	70.26	(0.6015,0.3816)
1-$Eu_{50\%}Tb_{50\%}$	50:50	50.41	49.59	(0.6391,0.3506)
1-$Eu_{70\%}Tb_{30\%}$	70:30	69.72	30.28	(0.6567,0.3377)
1-$Eu_{90\%}Tb_{10\%}$	90:10	90.55	9.45	(0.6543,0.3306)

1-$Eu_{100\%}Tb_0$	100:0	100	0	(0.6627,0.3314)

Table S6 The lifetimes ($^5D_4$ of Tb^{3+}, $^5D_0$ of Eu^{3+}) and energy transfer efficiency (η) from Tb^{3+} to Eu^{3+} for **1-Eu_xTb_{1-x}**.

1-Eu_xTb_{1-x}	$^5D_4$ of Tb^{3+} (ms)	$^5D_0$ of Eu^{3+} (ms)	η
1-$Eu_0Tb_{100\%}$	1.039	—	—
1-$Eu_{1\%}Tb_{99\%}$	0.854	1.202	0.178
1-$Eu_{2\%}Tb_{98\%}$	0.735	1.112	0.293
1-$Eu_{3\%}Tb_{97\%}$	0.645	1.093	0.379
1-$Eu_{4\%}Tb_{96\%}$	0.589	0.958	0.433
1-$Eu_{5\%}Tb_{95\%}$	0.533	0.913	0.487
1-$Eu_{6\%}Tb_{96\%}$	0.512	0.857	0.507
1-$Eu_{7\%}Tb_{93\%}$	0.492	0.784	0.527
1-$Eu_{8\%}Tb_{92\%}$	0.480	0.747	0.538
1-$Eu_{9\%}Tb_{91\%}$	0.485	0.701	0.533
1-$Eu_{10\%}Tb_{90\%}$	0.479	0.688	0.539
1-$Eu_{30\%}Tb_{70\%}$	0.453	0.660	0.564
1-$Eu_{50\%}Tb_{50\%}$	0.426	0.623	0.590
1-$Eu_{70\%}Tb_{30\%}$	0.341	0.672	0.672
1-$Eu_{90\%}Tb_{10\%}$	0.257	0.647	0.753
1-$Eu_{100\%}Tb_0$	—	0.566	—

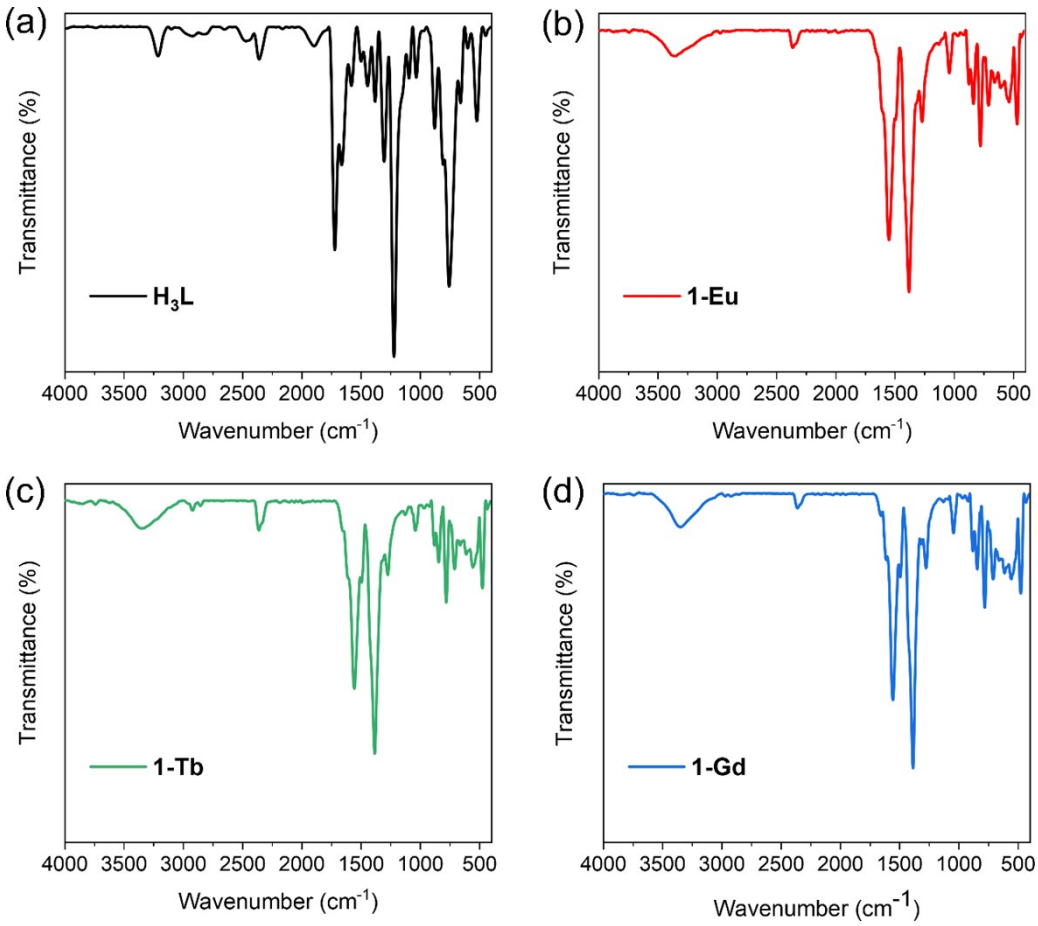

Fig. S1 The IR spectra: (a) H_3L; (b) **1-Eu**; (c) **1-Tb**; (d) **1-Gd**.

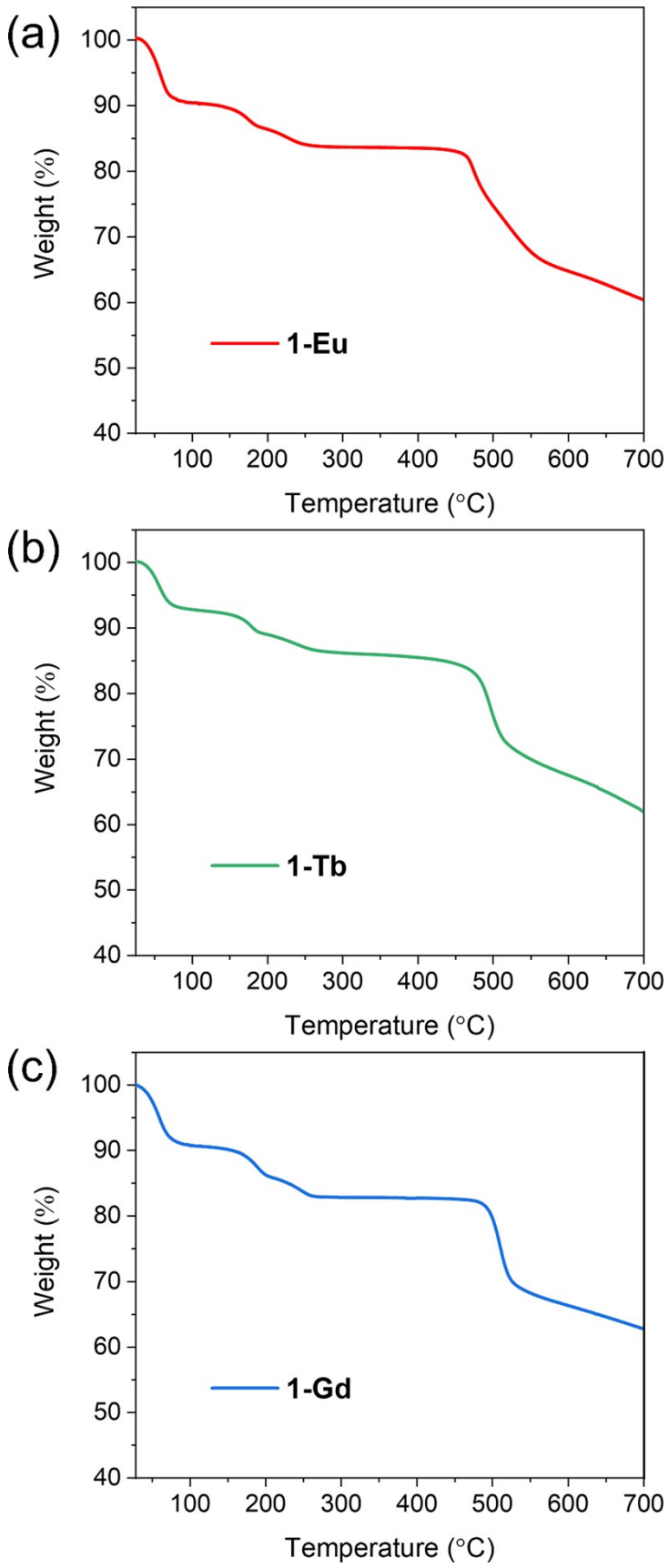

Fig. S2 Thermogravimetric analysis of **1-Eu** (a)**, 1-Tb** (b) and **1-Gd** (c).

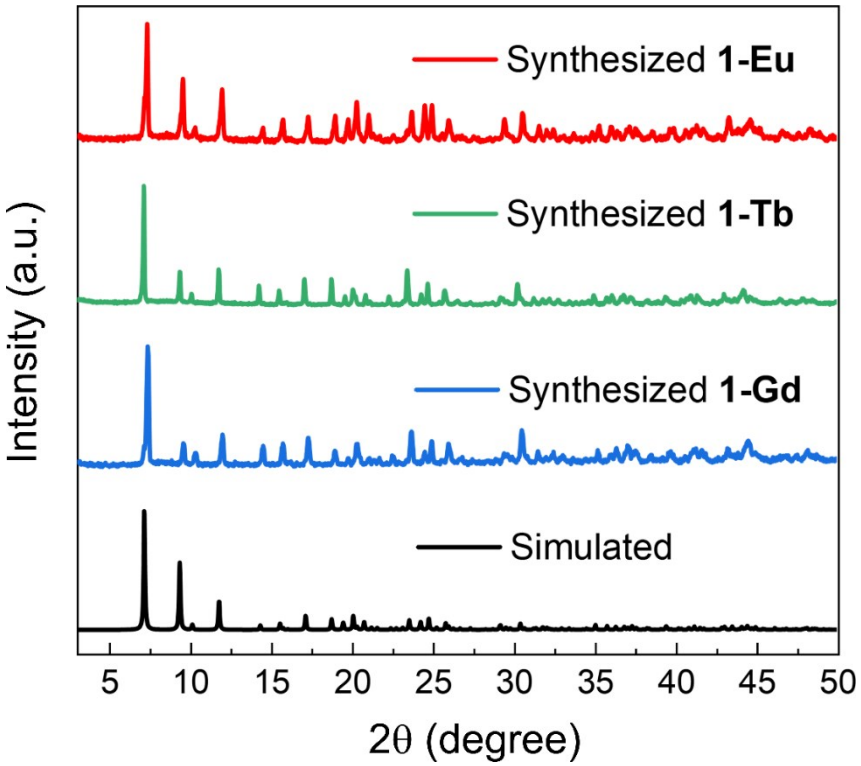

Fig. S3 PXRD patterns of **1-Eu, 1-Tb** and **1-Gd**.

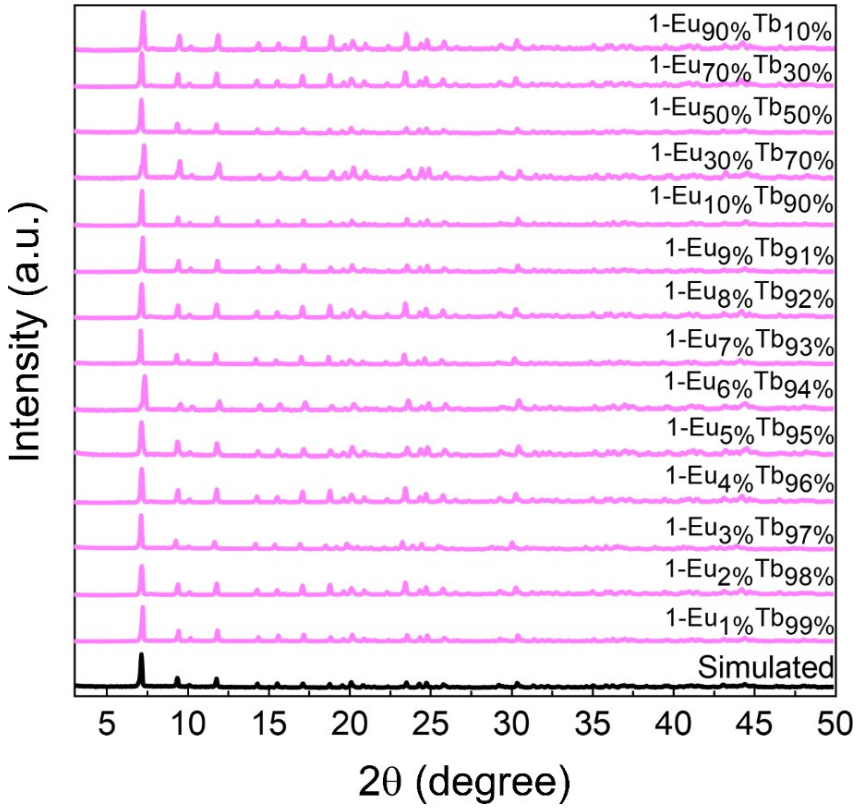

Fig. S4 PXRD patterns of **1-Eu_xTb_{1-x}**.

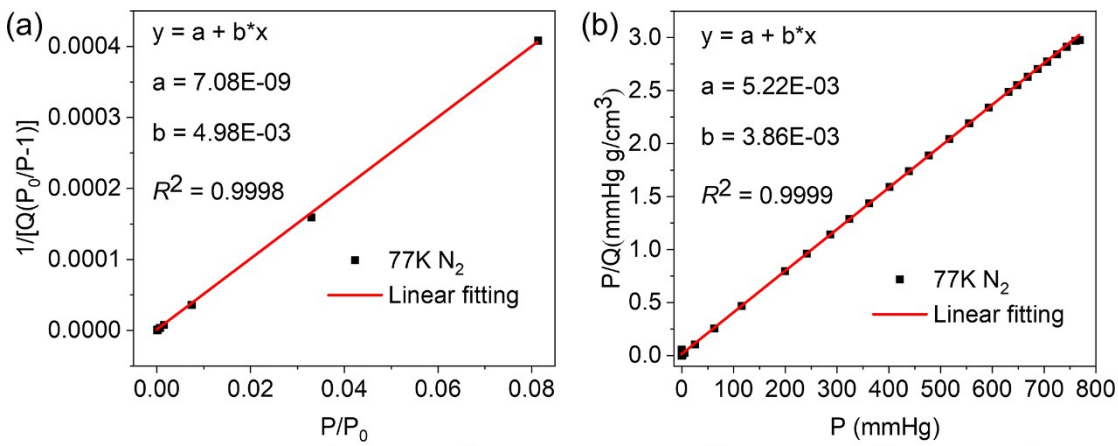

S_{BET} =1/(4.98×10^{-3}+7.08×10^{-9})/22414×6.023×10^{23}×0.162×10^{-18} = 873.3 m^2/g

$S_{Langmuir}$ = (1/0.00386)/22414×6.023×10^{23}×0.162×10^{-18} = 1128 m^2/g

Fig. S5 BET surface area plot (a), and Langmuir surface area plot (b) for **1-Eu-a.**

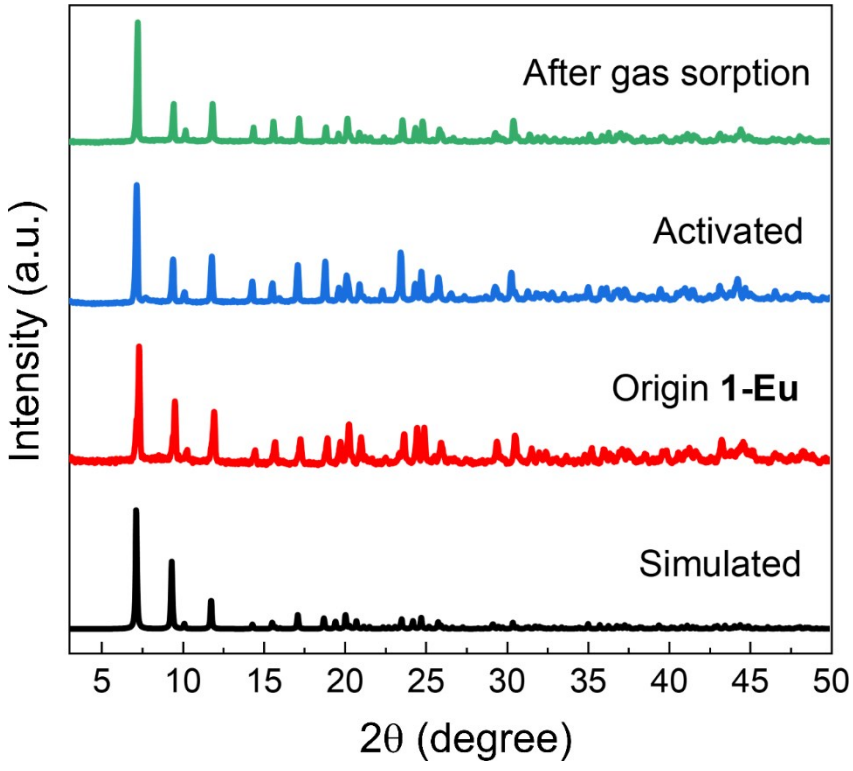

Fig. S6 PXRD patterns of **1-Eu,** activated **1-Eu** (**1-Eu-a**), and **1-Eu-a** after gas sorption.

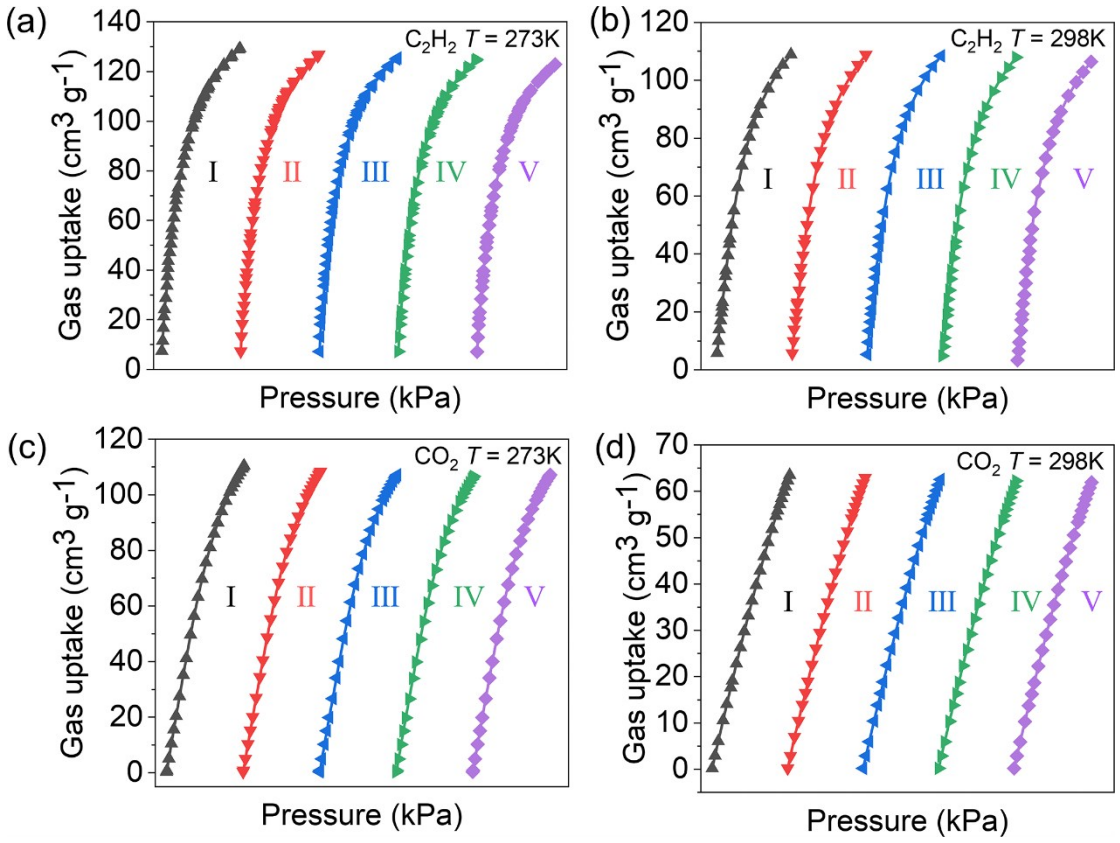

Fig. S7 (a, b) Repeated C_2H_2 adsorption isotherm of 5 cycles at 273 and 298K. (c, b) Repeated CO_2 adsorption isotherm of 5 cycles at 273 and 298K.

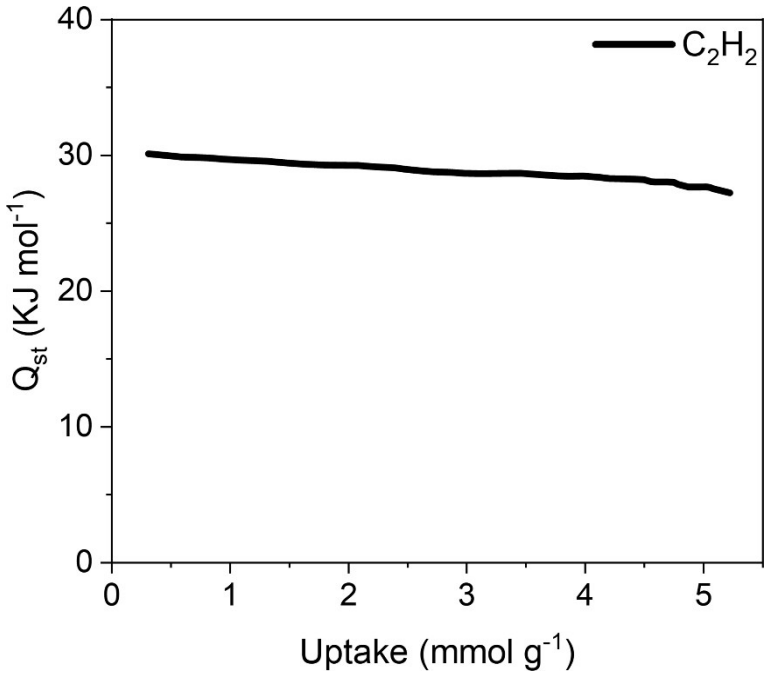

Fig. S8 The C_2H_2 adsorption enthalpies of **1-Eu-a**.

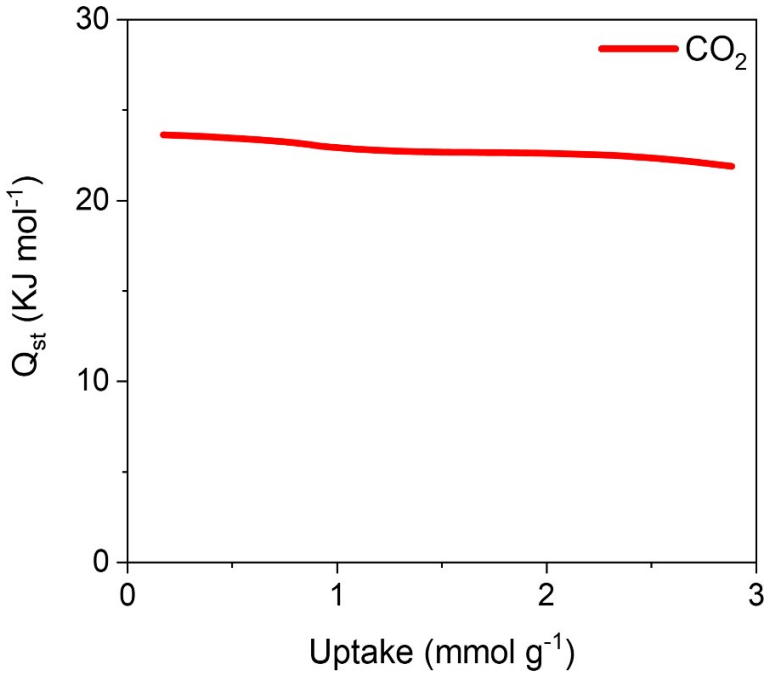

Fig. S9 The CO_2 adsorption enthalpies of **1-Eu-a**.

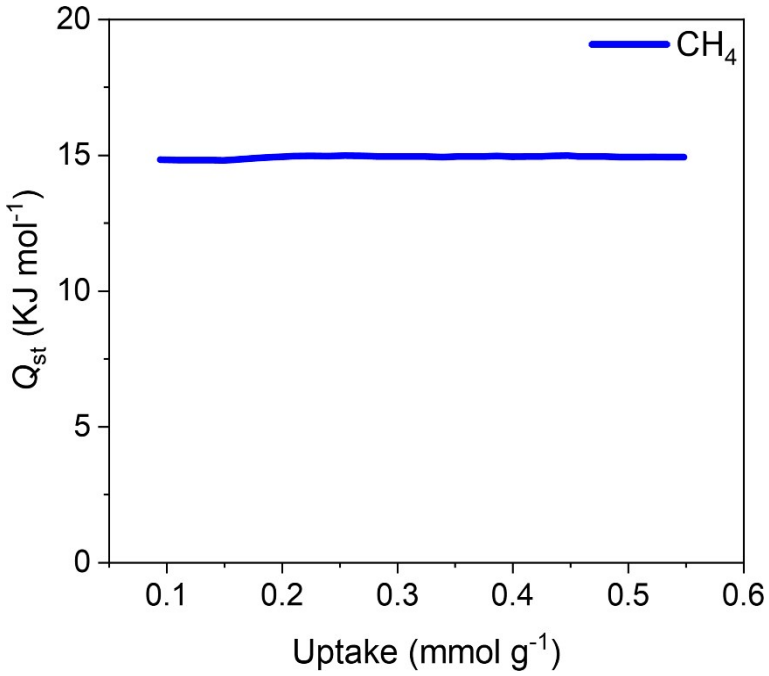

Fig. S10 The CH_4 adsorption enthalpies of **1-Eu-a**.

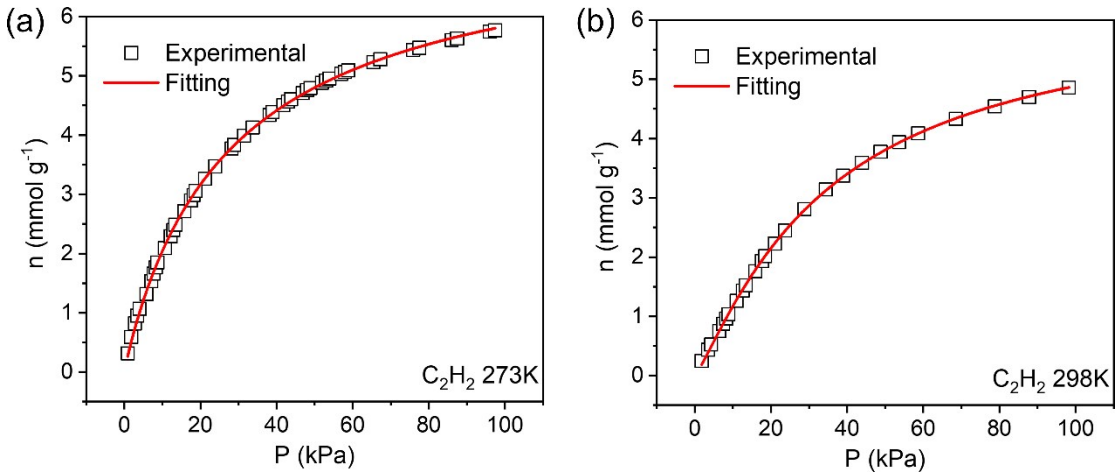

Fig. S11 DSLF fitting of the C_2H_2 adsorption isotherm of **1-Eu-a** at 273 K and 298K.

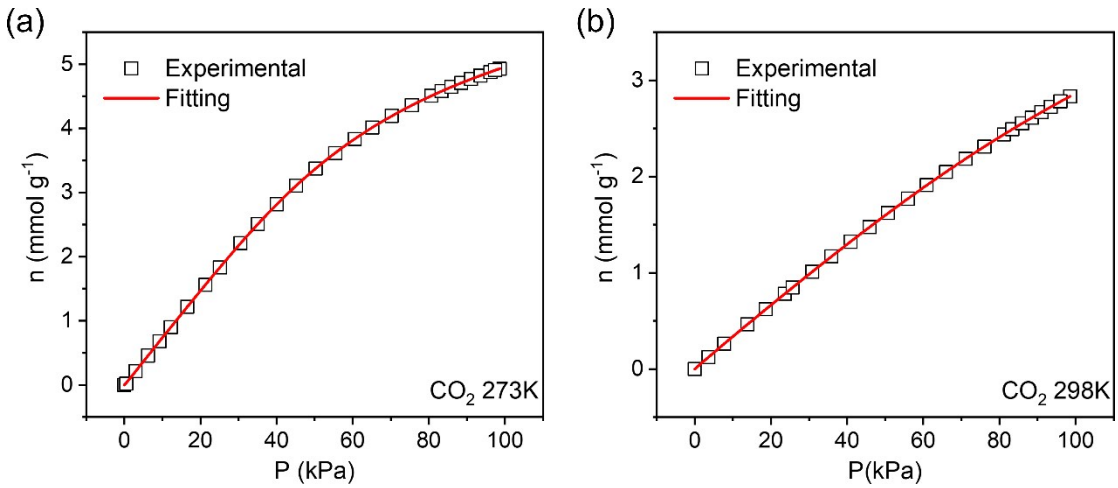

Fig. S12 DSLF fitting of the CO_2 adsorption isotherm of **1-Eu-a** at 273 K and 298K.

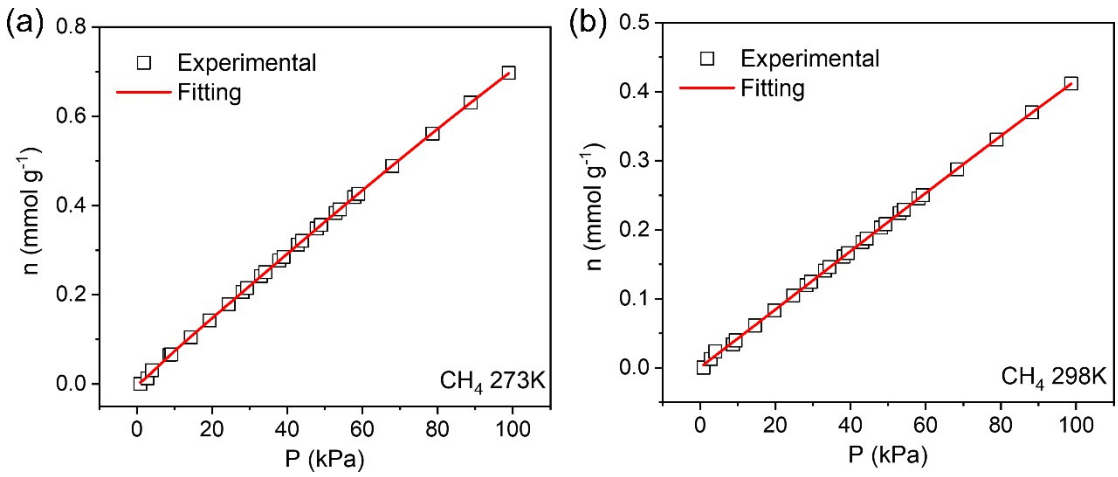

Fig. S13 DSLF fitting of the CH_4 adsorption isotherm of **1-Eu-a** at 273 K and 298K.

Table S7. DSLF parameters from the fitting of C_2H_2 adsorption isotherms of **1-Eu-a** at 273K and 298 K.

Parameter	273K	298K
q_{m1} (mmol g^{-1})	3.77884	3.14261
b_1 (kPa^{-1})	0.04027	0.01502
t_1	1.03831	0.84517
q_{m2} (mmol g^{-1})	3.77623	3.14172
b_2 (kPa^{-1})	0.04028	0.01502
t_2	1.03833	0.84519
R^2	0.9995	0.9998

Table S8. DSLF parameters from the fitting of CO_2 adsorption isotherms of **1-Eu-a** at 273K and 298 K.

Parameter	273K	298K
q_{m1} (mmol g^{-1})	1.32272	1.46671
b_1 (kPa^{-1})	0.0000488	0.0000826
t_1	0.38589	0.49271
q_{m2} (mmol g^{-1})	6.32952	5.85186
b_2 (kPa^{-1})	0.01074	0.00594
t_2	0.93304	1.00505
R^2	1	0.9999

Table S9. DSLF parameters from the fitting of CH_4 adsorption isotherms of **1-Eu-a** at 273K and 298 K.

Parameter	273K	298K
q_{m1} (mmol g^{-1})	3.58178	1.05157
b_1 (kPa^{-1})	0.00103	0.000514
t_1	0.85182	0.76639
q_{m2} (mmol g^{-1})	0.03292	8.1901
b_2 (kPa^{-1})	0.02824	0.000511
t_2	0.58708	1.13558
R^2	0.9999	0.9997

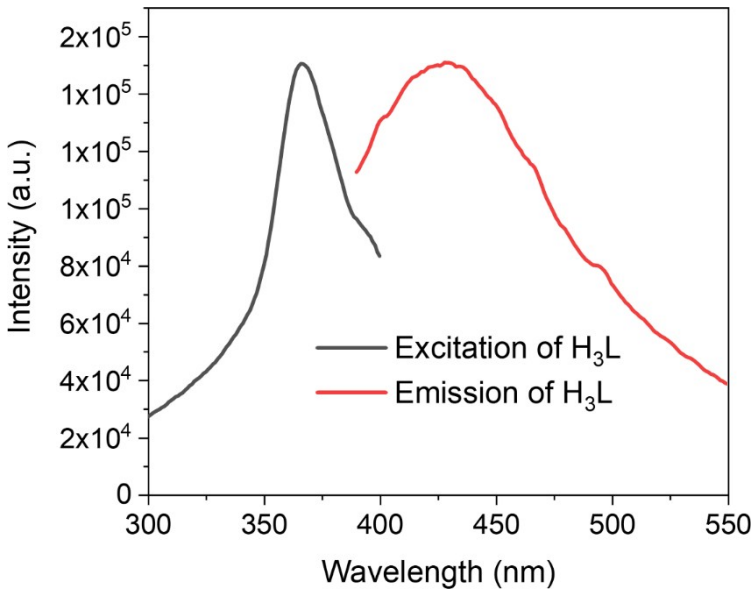

Fig. S14 Excitation and emission spectra of H_3L.

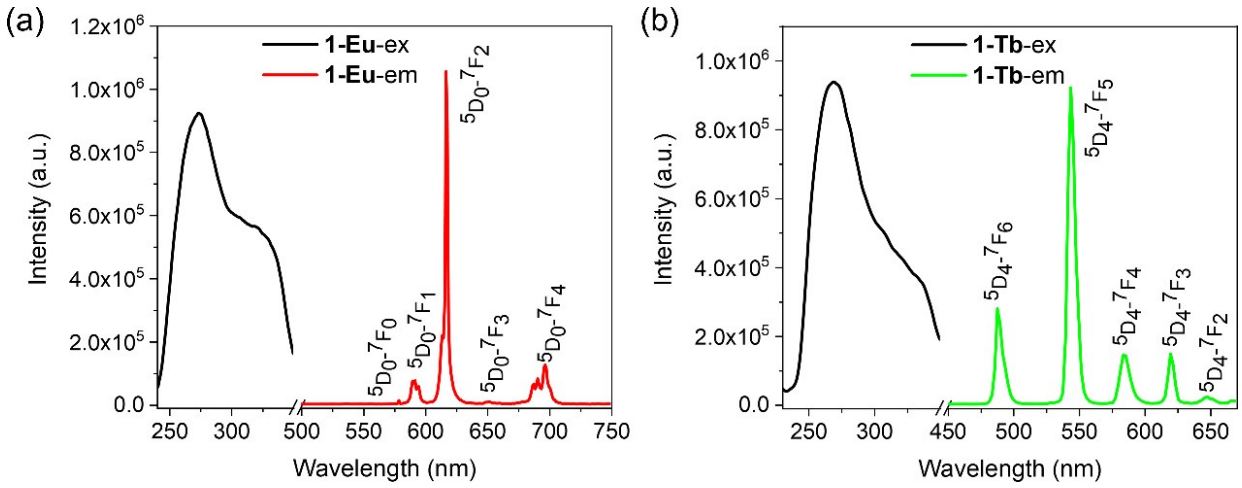

Fig. S15 Excitation and emission spectra of **1-Eu** (a) and **1-Tb** (b).

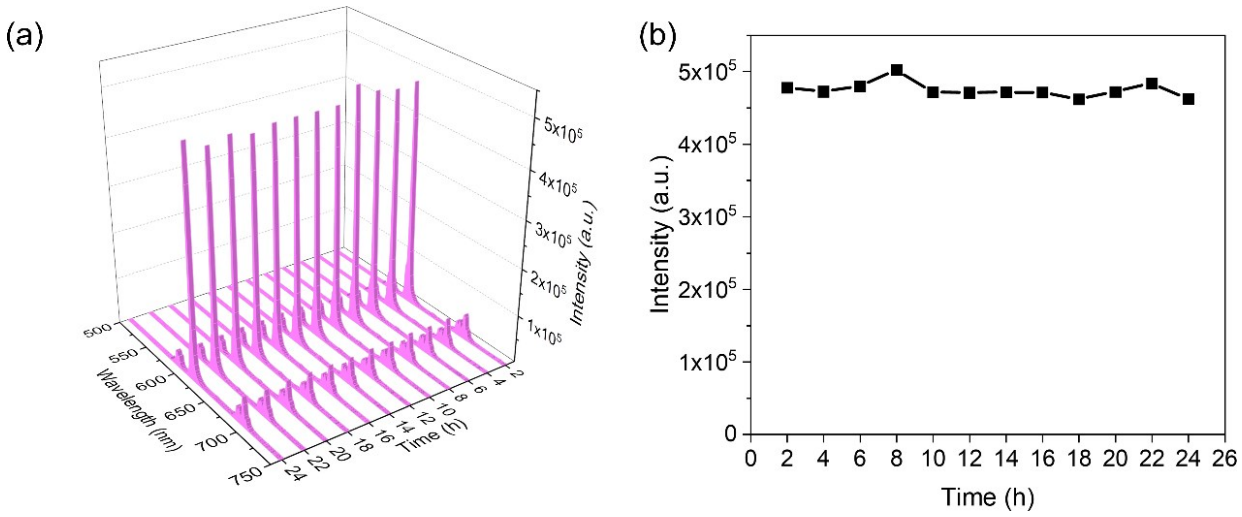

Fig. S16 Luminescence spectra (a) and emission intensities at 617nm (b) of **1-Eu** after immersion in water for different times.

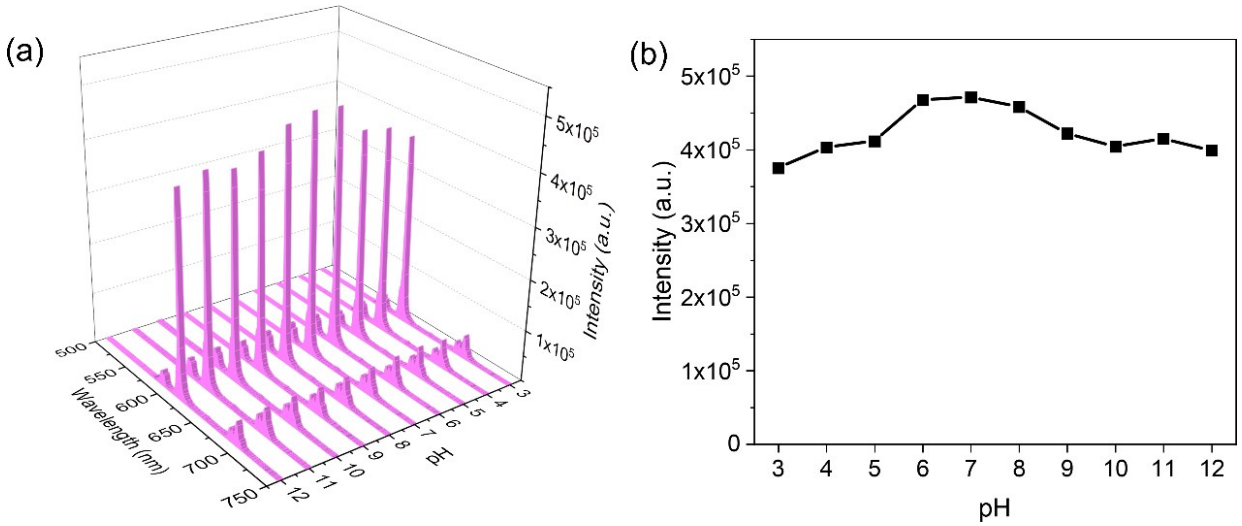

Fig. S17 The emission spectra (a) and emission intensities at 617nm (b) of **1-Eu** in aqueous solutions with different pH values (3-12).

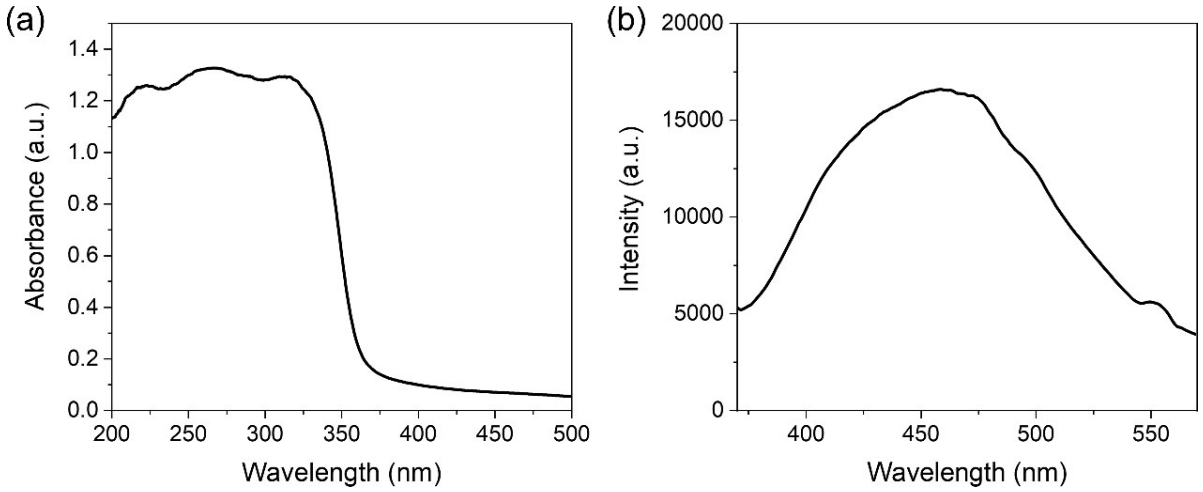

Fig. S18 (a) UV-vis absorption spectra of ligand H_3L. (b) The phosphorescence spectrum of **1-Gd** at 77 K.

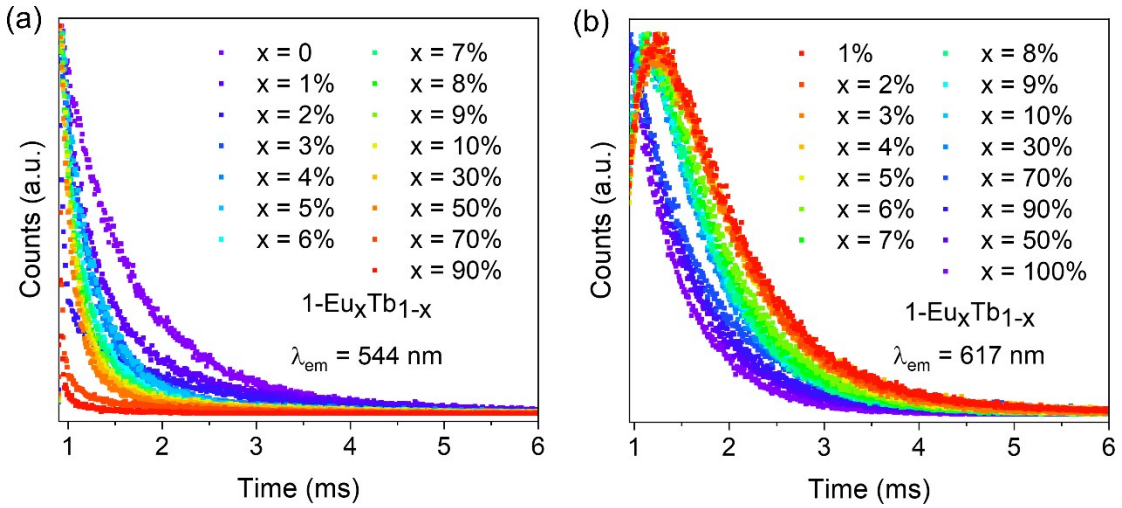

Fig. S19 Luminescent decay curves of **1-Eu_xTb_{1-x}**. (a) λ_{ex} = 280 nm, λ_{em} = 544 nm (b) λ_{ex} = 280 nm, λ_{em} = 617 nm.

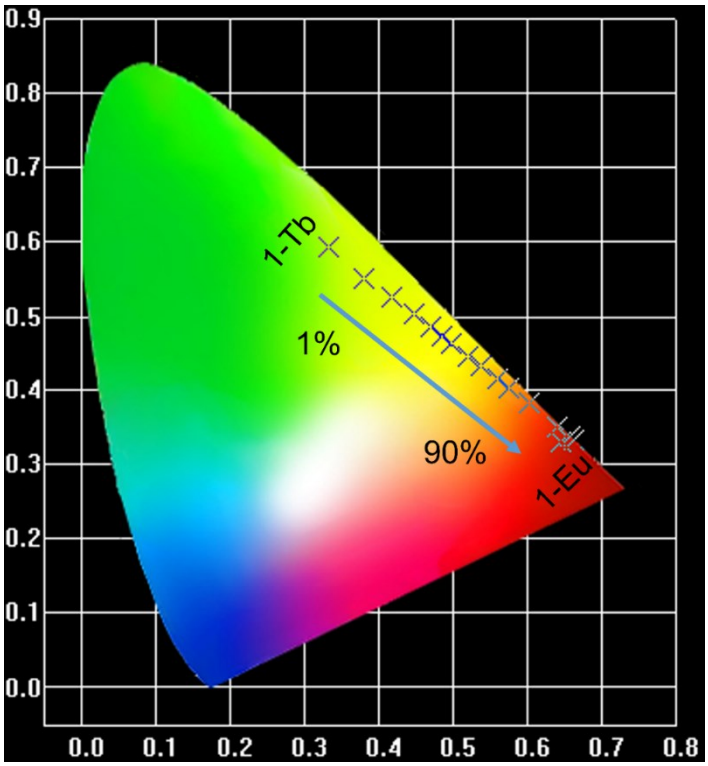

Fig. S20 CIE chromaticity diagram of doped **1-Eu$_x$Tb$_{1-x}$**.

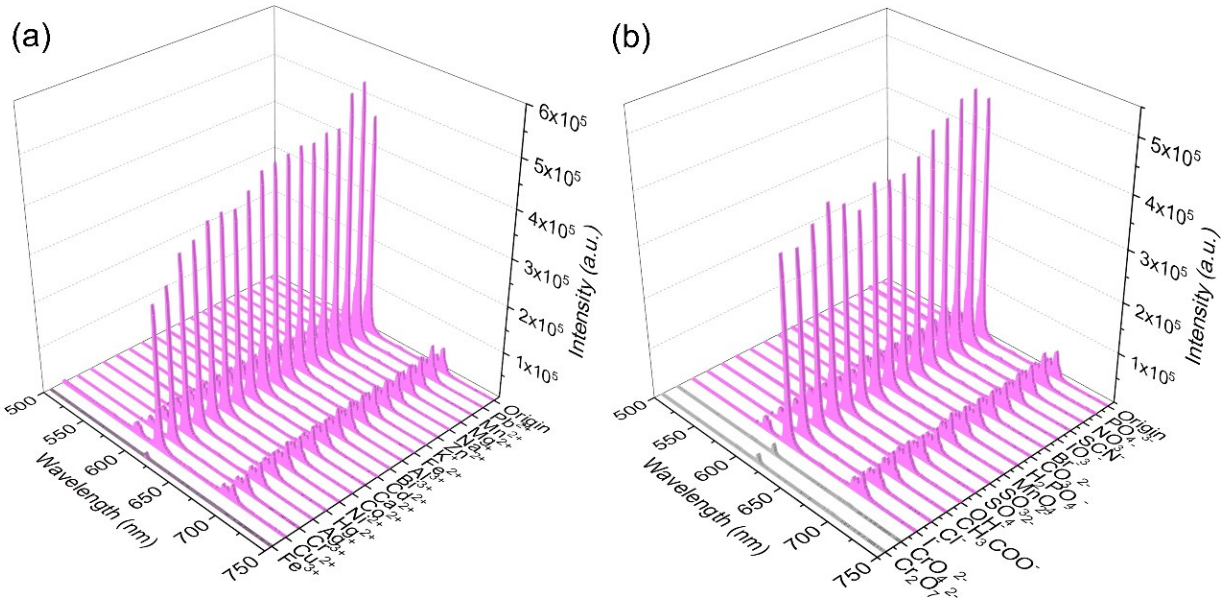

Fig. S21 Emission spectra of **1-Eu** immersed in cation and anion aqueous solutions.

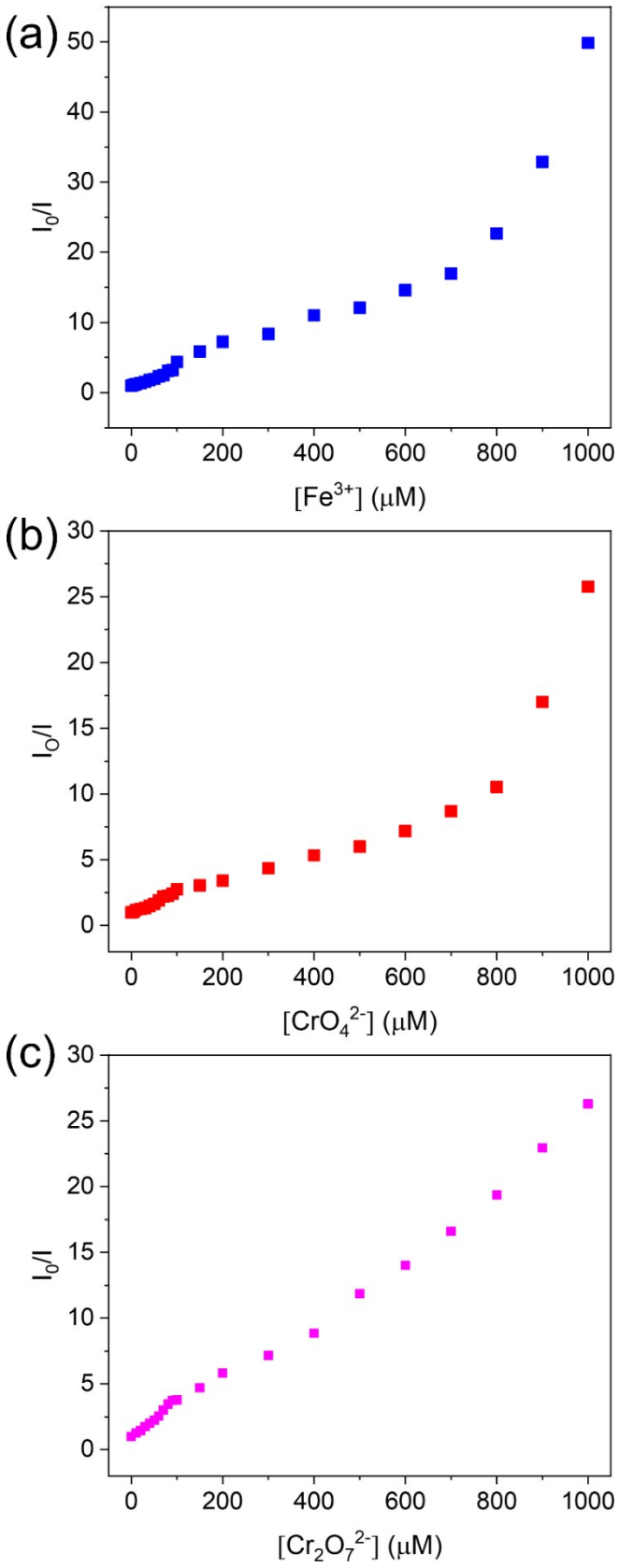

Fig. S22 Stern−Volmer plots for (a) Fe^{3+}, (b) CrO_4^{2-} and (c) $Cr_2O_7^{2-}$ in water suspensions of **1-Eu** (0−1000 μM).

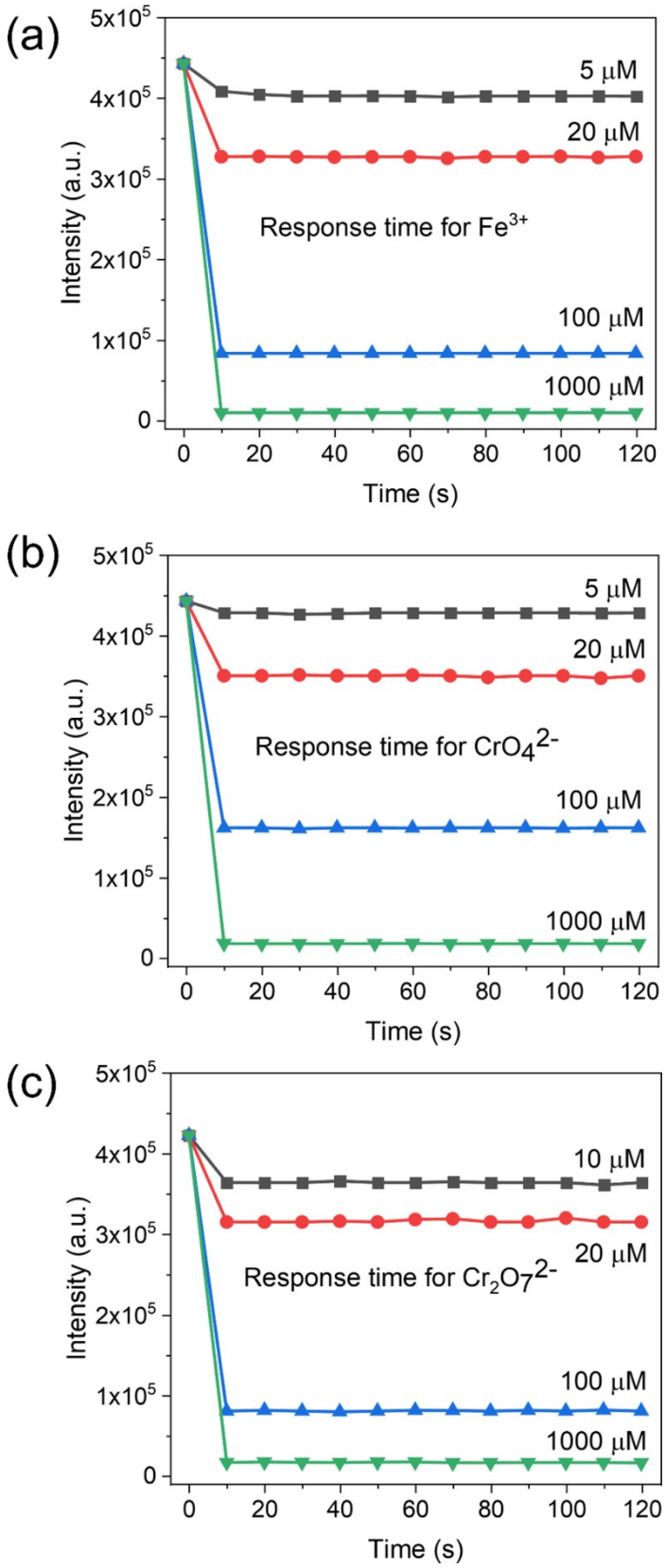

Fig. S23 Effects of response time on the fluorescent intensities at 617 nm of the aqueous suspension of **1-Eu** in the presence of Fe^{3+} (a), CrO_4^{2-} (b) and $Cr_2O_7^{2-}$ (c) at different concentrations.

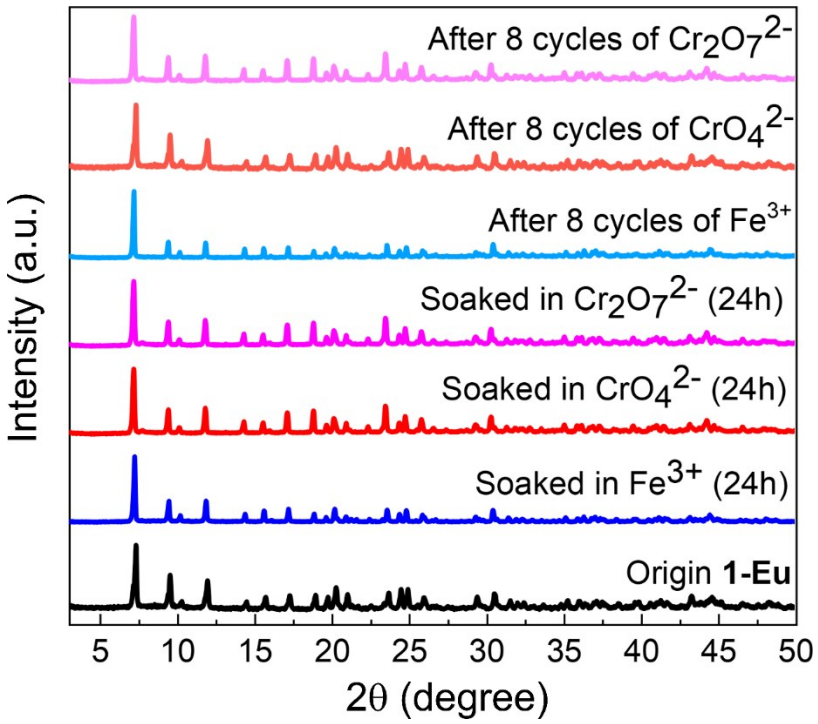

Fig. S24 The PXRD patterns of **1-Eu** after using eight cycles and soaked in aqueous Fe^{3+} and $CrO_4^{2-}/Cr_2O_7^{2-}$ solution (1 mM) for 24 h.

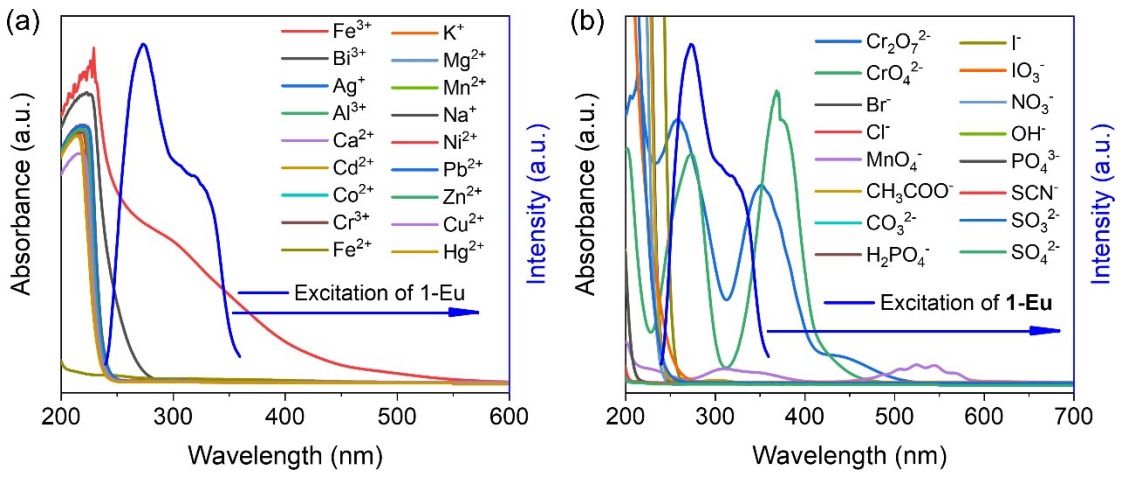

Fig. S25 The UV–Vis absorption spectrum of aqueous solutions of different testing cations (a), anions (b) and the excitation for **1-Eu**.

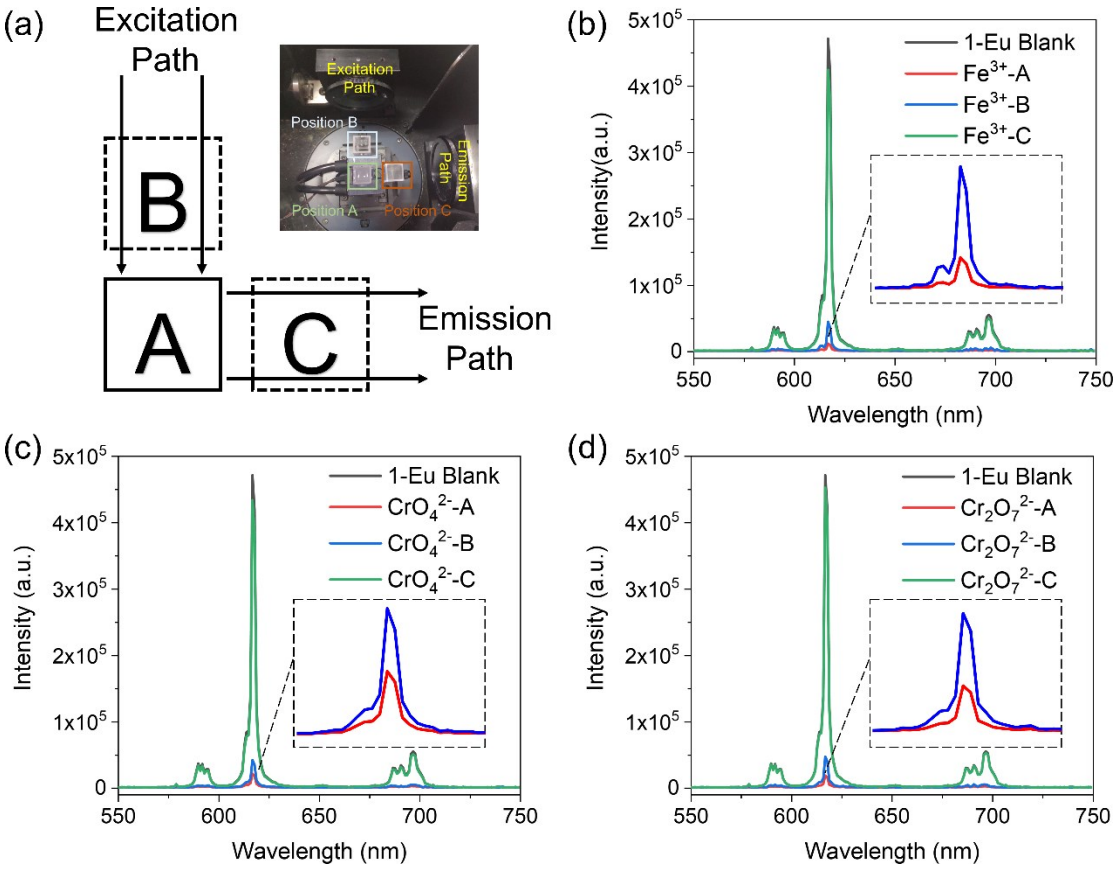

Fig. S26 (a) Schematic of the luminescent quenching mechanism experiment. The emission spectra of **1-Eu** (excited at 280 nm) with (b) Fe^{3+}, (c) CrO_4^{2-}, and (d) $Cr_2O_7^{2-}$. (Black curves, **1-Eu** solely in position A; red curves, mixture of **1-Eu** and Fe^{3+} and CrO_4^{2-}/$Cr_2O_7^{2-}$ ions in position A; blue curves, **1-Eu** in position A while Fe^{3+} and CrO_4^{2-}/$Cr_2O_7^{2-}$ ions in position B; green curves, **1-Eu** in position A while Fe^{3+} and CrO_4^{2-}/$Cr_2O_7^{2-}$ ions in position C.)

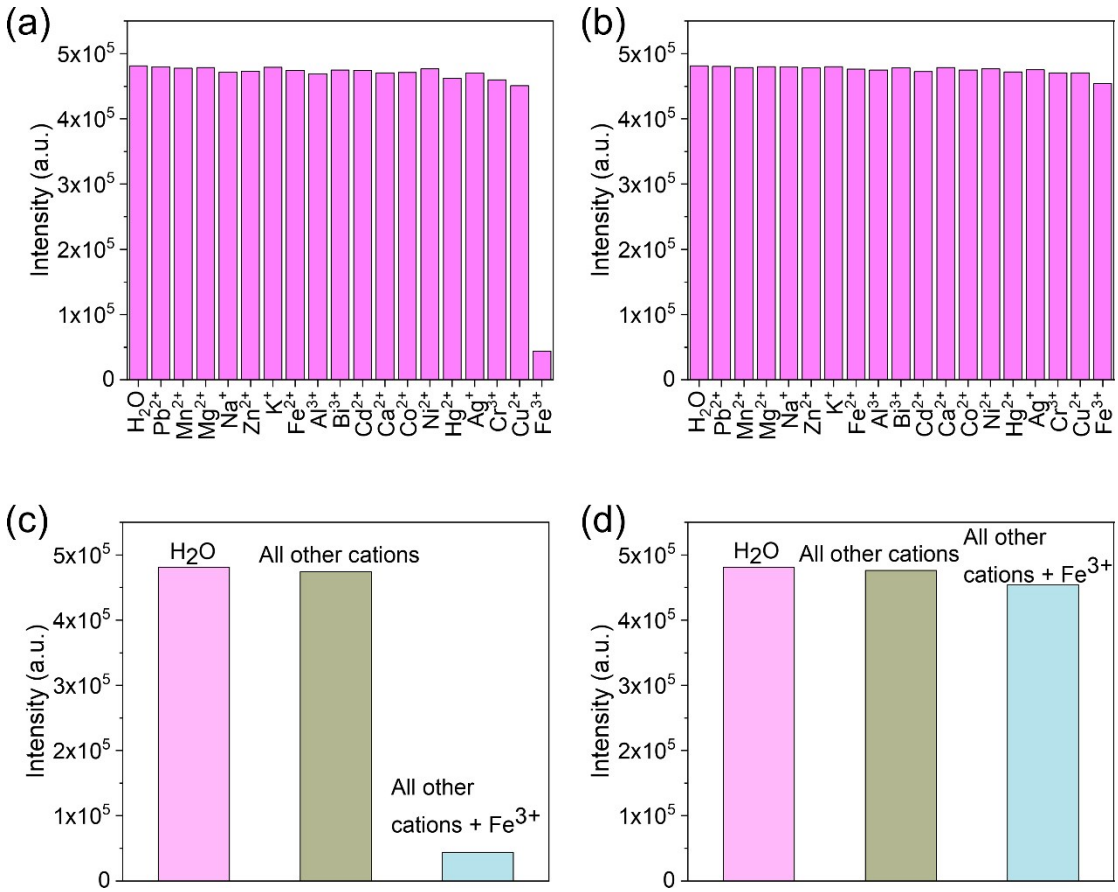

Fig. S27 The emission intensity of **1-Eu** at 617 nm with different testing cations placed in the excitation path (a, c) and emission path (b, d).

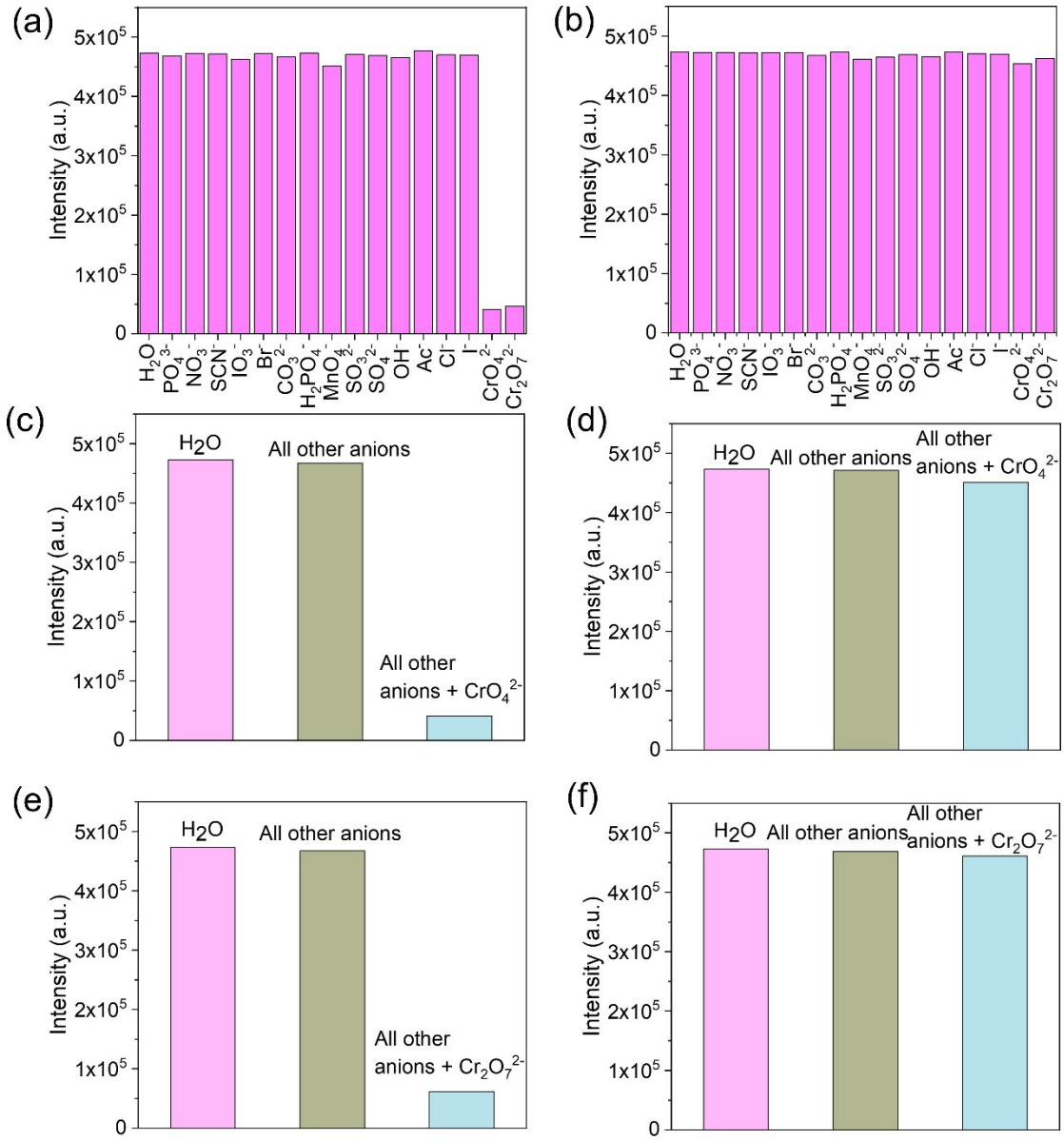

Fig. S28 The emission intensity of **1-Eu** at 617 nm with different testing anions placed in the excitation path (a, c, e) and emission path (b, d, f).

Table S10. A comparison of quenching constants and corresponding LODs for various luminescent MOFs used for detection of Fe^{3+}.

Materials	solvent	$K_{sv}(M^{-1})$	Detection limit (μM)	Reference
534-MOF-Tb(L_{11})	water	5.51×10^3	130	10
$[Cd(NDA)(L)(H_2O)_2]_n$	water	4.0×10^4	2.06	11
BUT-15	water	1.66×10^4	0.3	12
$[Zn_2(TPOM)(NDC_)2]3.5H_2O$	water	1.9×10^4	2	13
IISERP-MOF25	water	1.52×10^4	12.3	14

$[Eu(L)(H_2O)]\cdot 1.5H_2O$	water	6.6×10^4	0.87	15
FJI-C8 (Zn)	water	8.2×10^3	23.3	16
$\{[Cd_2(bptc)(phen)_2]\cdot 4H_2O\}n$	water	3.07×10^3	21.7	17
$Eu_2(MFDA)_2(HCOO)_2(H_2O)_6$	DMF	1.58×10^3	0.3	18
MOF-808-Tb	water	3.12×10^4	—	19
$[Ln(L_2)(H_2O)(DMF)]_n$	water	3.10×10^4	1.57	20
[Eu(O-cpia)(phen)]	water	—	300 ppm	21
$[Zr_6O_4(OH)_4(C_8H_2O_4S_2)_6]\cdot DMF\cdot 18H_2O$	water	4.41×10^3	1.26	22
DPYBT	water	—	3.04	23
$[Cd_2Na(L_{15})(BDC)_{2.5}].9H_20$	DMF	1.67×10^4	162ppb	24
$\{[Cd(5\text{-}asba)(bimb)]\}_n$	water	1.78×10^4	—	25
1-Eu	water	1.88×10^4	0.57	This work

Table S11. A comparison of quenching constants and corresponding LODs for various luminescent MOFs used for detection of $CrO_4^{2-}/Cr_2O_7^{2-}$.

Materials	Analytes	solvent	Detection limit (μM)	Reference
$[(CH_3)_2NH_2][In(TNB)_{4/3}]\cdot(2DMF)(3H_2O)$	CrO_7^{2-}	water	45	26
$[Zn_2(L_1)(L_2)_2]\cdot 4H_2O$	CrO_4^{2-}/CrO_7^{2-}	DMF	4.8/3.9	13
$\{[Zn_3(mtrb)_3(btc)_2]\cdot 3H_2O\}_n$	CrO_4^{2-}/CrO_7^{2-}	water	4.52/2.83	27
$[Zn(NH_2\text{-}bdc)(4,4'\text{-}bpy)]$	CrO_4^{2-}/CrO_7^{2-}	water	2.21/1.3	28
$[Zn(tpbpc)_2]\cdot$solvent	CrO_4^{2-}/CrO_7^{2-}	water	0.47 / 0.68	29
$Zr_6O_4(OH)_7(H_2O)_3(btba)_3$	CrO_7^{2-}	water	1.57	30
$[Zn_3(bpanth)(oba)_3]\cdot 2DMF$	CrO_4^{2-}/CrO_7^{2-}	water	2.67/1.85	31
$[Eu_7(mtb)_5(H_2O)_{16}](NO_3)(DMA)_8(H_2O)_{18}$	CrO_4^{2-}	water	3.5 nM	32
$[Cd(TIPA)_2(ClO_4)_2](DMF)_3(H_2O)$	CrO_7^{2-}	water	27nM	33
Eu^{3+}@MIL-124	CrO_7^{2-}	water	0.15	34
NU-1000	CrO_7^{2-}	water	1.8	35
$\{[Zn_2L_2(H_2O)_4]\cdot H_2O\}_n$	CrO_4^{2-}/CrO_7^{2-}	water	2.3 / 2.6	36
USTC-5	CrO_4^{2-}/CrO_7^{2-}	water	11.4/1.45	37
Zn-MOF-1	CrO_4^{2-}/CrO_7^{2-}	water	4.8/3.53	38
1-Eu	CrO_4^{2-}/CrO_7^{2-}	water	0.79/0.42	This work

References

1 G. M. Sheldrick, Program for Empirical Absorption Correction of Area Detector Data, University of Göttingen, Germany, 1996.

2 G. M. Sheldrick, SHELXS-97, Program for Crystal Structure Solution, Göttingen University, Göttingen, Germany, 1997.

3 H. Pan, J. A. Ritter and P. B. Balbuena, *Langmuir,* 1998, **14**, 6323-6327.

4 B. Li, Y. Zhang, R. Krishna, K. Yao, Y. Han, Z. Wu, D. Ma, Z. Shi, T. Pham, B. Space, J. Liu, P. K. Thallapally, J. Liu, M. Chrzanowski and S. Ma, *J. Am. Chem. Soc.*, 2014, **136**, 8654–8660.

5 A. L. Myers and J. M. Prausnitz, *AIChE J.*, 1965, **11**, 121-127.

6 G. Kresse and J. Furthmuller, *Comput. Mater. Sci.*, 1996, **6**, 15-50.

7 P. E. Blöchl, *Phys. Rev. B* 1994, **50**, 17953-17979.

8 J. P. Perdew, J. A. Chevary, S. H. Vosko, K. A. Jackson, M. R. Pederson, D. J. Singh and C. Fiolhais, *Phys. Rev. B: Condens. Matter Mater. Phys.,* 1992, **46**, 6671-6687.

9 S. Grimme, J. Antony, S. Ehrlich and H. Krieg, *J. Chem. Phys.,* 2010, **132**, 154104.

10 M. Chen, W. M. Xu, J. Y. Tian, H. Cui, J. X. Zhang, C. S. Liu and M. Du, *J. Mater. Chem. C.*, 2017, **5**, 2015-2021.

11 J. F. Zhang, S. M. Ren, H. C. Xia, W. Jia and C. Zhang, *J. Mater. Chem. C,* 2020, **8**, 1427-1432.

12 B. Wang, Q. Yang, C. Guo, Y. Sun, L. H. Xie and J. R. Li, *ACS Appl. Mater. Interfaces*, 2017, **9**, 10286-10295.

13 R. Lv, J. Y. Wang, Y. P. Zhang, H. Li, L. Y. Yang, S. Y. Liao, W. Gu and X. Liu, *J. Mater. Chem. A*, 2016, **4**, 15494-15500.

14 R. Maity, D. Chakraborty, S. Nandi, A. K. Yadav, D. Mullangi, C. P. Vinod and R. Vaidhyanathan, *ACS Appl. Nano Mater*, 2019, **2**, 5169-5178.

15 Y. Tao, P. Zhang, J. Liu, X. Chen, X. Guo, H. Jin, J. Chai, L. Wang and Y. Fan, *New. J. Chem.*, 2018, **42**, 19485-19493.

16 C. H. Chen, X. S. Wang, L. Li, Y. B. Huang and R. Cao, *Dalton Trans.,* 2018, **47**, 3452-3458.

17 Y. Lin, X. Zhang, W. Chen, W. Shi and P. Cheng. *Inorg. Chem.* 2017, **56**, 11768-11778.

18 X. H. Zhou, L. Li, H. H. Li, A. Li, T. Yang and W. Huang, *Dalton Trans.* 2013*,* **42***,* 12403-12409.

19 J. Zhang, S. B. Peh, J. Wang, Y. H. Du, S. B. Xi, J. Q. Dong, A. Karmakar, Y. P. Ying, Y. X. Wang and D. Zhao, *Chem. Commun.,* 2019, **55**, 4727-4730.

20 X. N. Mi, D. F. Sheng and S. N. Wang, *ACS Appl. Mater. Interfaces,* 2019, **11**, 7914-7926.

21 Q. S. Wang, J. J. Li, M. N. Zhang and X. Li, *Sens. Actuators, B.,* 2018, **258**, 358-364.

22 R. Dalapati, Ü. Kökçam-Demir, C. Janiak and S. Biswas, *Dalton Trans.,* 2018, **47**, 1159-1170.

23 J. Qian, N. Huang, Q. Lu, C. Wen and J. Xia, *Sens. Actuators, B,* 2020, **320**. 128377-128386.

24 D. Zhao, X. H. Liu, Y. Zhao, P. Wang, Y. Liu, M. Azam, S. Al-Resayes, Y. Lu and W. Y. Sun, *J. Mater. Chem. A,* 2017, **5**, 15797-15807.

25 Y. J. Yang, M. J. Wang and K. L. Zhang, *J. Mater. Chem. C.*, 2016, **4**, 11404-11418.

26 H. R. Fu, Y. Zhao, T. Xie, M. L. Han, L. F. Ma and S. Q. Zang, *J. Mater. Chem. C.*, 2018, **6**, 6440–6448.

27 Y. Q. Zhang, V. A. Blatov, T. R. Zheng, C. H. Yang, L. L. Qian, K. Li, B. L. Li and B. Wu, *Dalton Trans.,* 2018, **47**, 6189–6198.

28 T. Wiwasuku, J. Boonmak, K. Siriwong, V. Ervithayasuporn and S. Youngme, *Sens. Actuators, B,* 2019, **284**, 403-413.

29 J. Xiao, J. Liu, X. Gao, G. Ji, D. Wang and Z. Liu, *Sens. Actuators, B,* 2018, **269**, 164-172.

30 T. He, Y. Z. Zhang, X. J. Kong, J. M. Yu, X. L. Lv, Y. F. Wu, Z. J. Guo and J. R. Li, *ACS Appl. Mater. Interfaces,* 2018, **10**, 16650-16659.

31 Z. Q. Yao, G. Y. Li, J. Xu, T. L. Hu and X. H. Bu, *Chem.-Eur. J.,* 2018, **24**, 3192-3198.

32 W. Liu, Y. L. Wang, Z. L. Bai, Y. X. Li, Y. X. Wang, L. H. Chen, L. Xu, J. Diwu, Z. F. Chai and S. A. Wang, *ACS Appl. Mater. Interfaces,* 2017, **9**, 16448-16457.

33 H. Fu, Y. Zhao, Z. Zhou, X. Yang and L. Ma, *Dalton Trans.,* 2018, **47**, 3725-3732.

34 X. Y. Xu and B. Yan, *ACS Appl. Mater. Interfaces,* 2015, **7**, 721-729.

35 Z. J. Lin, H. Q. Zheng, H. Y. Zheng, L. P. Lin, Q. Xin and R. Cao, *Inorg. Chem.,* 2017, **56**, 14178-14188.

36 C. X. Wang, Y. P. Xia, Z. Q. Yao, J. L. Xu, Z. Chang and X. H. Bu, *Dalton Trans.,* 2019, **48**, 387-394.

37 B. Li, Q. Yan and G. Yong, *J. Mater. Chem. C,* 2020, DOI: 10.1039/C9TC07030C.

38 X. Y. Guo, F. Zhao, J. J. Liu, Z. L. Liu and Y. Q. Wang, *J. Mater. Chem. A,* 2017, **5**, 20035-20043.